



# Computational investigation of magnetohydrodynamics Casson micropolar fluid flowing past a permeable linearly stretchy wall with heat source

S. Alao<sup>a</sup>, R. A. Oderinu<sup>a</sup>, B. A. Sanusi<sup>a,\*</sup>, T. A. Oyeyinka<sup>a</sup>, F. J. Ayanbukola<sup>a</sup>

<sup>a</sup>Department of Mathematics, Ladoko Akintola University of Technology, P.M.B 4000, Ogbomosho, Nigeria

## Abstract

In this study, a computational investigation that analyze the behavior of Magnetohydrodynamic (MHD) micropolar Casson fluid flowing via a linearly stretchy wall, considering the effects of heat source in a permeable medium. To achieve this, a similarity transformation is adopted, to convert the fundamental partial differential equations into nonlinear ordinary differential equations which are then solved numerically using collocating weighted residual scheme that adopts Hermite polynomials as the basis functions and Gauss-Lobatto points for spatial discretization. To affirm the accuracy of the simulation, the outputs are validated using 4th order Runge-Kutta method via shooting technique serving as the control method with the aid of Mathematical software (Maple 18.0). This approach enables the numerical solutions for the velocity  $\bar{f}'$ ; temperature  $\bar{\theta}$ , and microstructure  $\bar{g}$  of the fluid. The results are then presented in tabular and graphical forms, allowing for a detailed assessment of the impact of various parameters on the fluid's behavior. It is deduced that, increased porosity enhances thermal dispersion, reduces thermal resistance, and promotes heat transfer. Also, as magnetic field ( $M$ ) increases, the temperature profile exhibits significant enhancement, primarily as a result of viscous heating, resulting in improved temperature at the wall. As the viscous dissipation activity enhances, the heat profile also improves as a result of steady growth in the heat boundary layer. Through the comprehensive analysis of the graphical results, the relationship between these parameters and the fluid's behavior were properly observed, shedding light on the underlying physical mechanisms. This study establishes the influence of fluid mobility and Eckert number on thermal profiles, providing critical implications for industrial heat transfer optimization and fluid flow management and contributing to a depth understanding of the complex dynamics of MHD Casson fluid flow in porous media with potential applications in different fields of engineering and physics.

DOI:10.46481/jnsps.2025.2577

**Keywords:** Casson fluid, Porosity, Joule heating, Heating transfer, Hermite Collocation

## Article History :

Received: 19 December 2024

Received in revised form: 21 March 2025

Accepted for publication: 21 March 2025

2025-03-21 Published: 21 April 2025

© 2025 The Author(s). Published by the [Nigerian Society of Physical Sciences](#) under the terms of the [Creative Commons Attribution 4.0 International license](#). Further distribution of this work must maintain attribution to the author(s) and the published article's title, journal citation, and DOI.

Communicated by: P. Thakur

## 1. Introduction

Diverse applications of non-Newtonian fluid properties including everyday substances like shampoos, blood at low shear

rates, paints, apple sauce, sugar solutions, and muds, has sparked intense scientific interest in recent years. These fluids are characterized by their departure from Newtonian flow behavior, and examples of these fluids can be found naturally. In response, the academic community has developed and analyzed various mathematical models to understand and predict

\*Corresponding author Tel. No: +234-808-665-6590.  
Email address: [sanusib54@gmail.com](mailto:sanusib54@gmail.com) (B. A. Sanusi)

the behavior of these complex fluids, with many more models currently in development. Casson fluids, a subclass of non-Newtonian fluids have garnered significant attention and interest of researchers due to their unique rheological features and wide applications in fields like biomedical engineering, chemical processing, and petroleum industries. Marked by their remarkable shear thickening behavior and yield stress, Casson fluids exhibit intricate dynamics that continue to intrigue scientist. Despite substantial efforts, the flow behavior of Casson fluids remains enigma with numerous unanswered questions and challenges. Benazir *et al.* [1] conducted an experiment on Casson fluid flow between a vertical cone and flat plate with a non-uniform heat sink/source, finding that the flow became non-uniform as time progressed. Shaw *et al.* [2] investigated the effect of nonlinear heat convection on Casson fluid flow over a flat plate, revealing that the a higher Casson parameter resulted in a narrower momentum boundary layer. In his research, Sobomowo [3] analyzed the natural convection and heat transmission of Casson fluid flow through a vertical plate, with a particular emphasis on the influence of thermal radiation when nanoparticles are added. the study shows that the nanofluid's velocity and temperature increase as the radiation parameter grows. Hayat *et al.* [4] explored the consequences of a chemically reactive Casson fluid model on heat convection at a stretching surface, considering the effects of non-material flow. In their study, Haldar *et al.* [5] designed a dual-solution framework for understanding the mixed convection of casson fluid flow. Mustafa and Khan [6] examined the flow of Casson nanofluids using a general power law velocity distribution. Similarly, Sarkar and Endalew [7] considered the progression of Casson nanofluids in relation to wedge angle aggregation and melting processes. The flow of Casson nanofluids through single and multiple walled carbon nanotubes, incorporating chemical reactions was investigated by Ibrar *et al.* [8]. Furthermore, several researchers have recently developed dynamic models that incorporate diverse flow features to better understand the complexities of Casson fluids. (see Refs. ([9–15])).

The interplay between magnetic fields, electrically conducting fluids, and temperature gradients has a profound impact on heat transfer, giving rise to several key effects. Notably, the induced fluid motion and mixing can significantly enhance heat transfer rates, altering temperature distribution and convective heat transfer. Furthermore, this complex interaction affects the formation and growth of thermal boundary layers, influencing heat transfer. the generated electrical currents can also result to Joule heating, further impacting temperature fields, this situation can be leveraged to augment heat transfer in various applications, like heat exchangers and thermal management systems. Understanding the influence of this interplay on heat transfer is crucial for designing and optimizing systems containing electrically conducting fluids, magnetic fields, and heat transfer, including fusion reactors, electromagnetic pumps, and MHD generators.

Magnetohydrodynamics(MHD) explores the dynamic interplay between magnetic fields and electrically conducting fluids, where the magnetic field can trigger an electric current, then, produces a Lorentz force that influences the fluid's flow

behavior. With its far-reaching implications, MHD flow has numerous practical applications across various fields, such as power generation, materials processing, and space exploration, making it a vital area of study [16–21] In certain power plants, Magnetohydrodynamics(MHD) generators are used to convert heat energy into electrical power [22]. MHD technology is employed in materials processing to control and direct the flow behavior of fluids using pumps and mixers [23]. In space exploration, MHD thrusters are used to maneuver and propel spacecraft with precision [24]. Accurate modeling and understanding of MHD flow behavior is crucial for enhancing the design and operational efficiency of processes in these industries. To address this, recent study has concentrated on creating innovative numerical methods and experimental approaches to investigate the intricate dynamics of MHD systems, ultimately aiming to improve their performance and applicability. Kumar *et al.* [25] carried out a study on the impact of Hall current on MHD flow within a channel featuring porous walls, revealing that the Hall current has a profound influence on the flow dynamics, leading to notable changes in its behavior. In their study, Bojarevics *et al.* [26] established a numerical framework to simulate MHD flow in liquid metal batteries, emphasizing the significance of accurate magnetic field representation in reproducing realistic flow patterns. Katarina *et al.* [27] conducted a comprehensive study to investigate the effects of chemical and radiation reactions on the Magnetohydrodynamics(MHD) flow of Casson fluid, which was induced by an oscillating vertical plate embedded in a porous medium. Their research aimed to elucidate the complex relationships between these reactions and the fluid's flow behavior in this specific setting. Metan *et al.* [28] examined the influence of a first-order chemical reaction on MHD flow across an infinite vertical plate, considering variable mass diffusion and exponential thermal radiation effects. Baagi *et al.* [29] investigated the impact of chemical reactions, heat generations/absorption, and induced magnetic fields on the steady magnetohydrodynamics(MHD) mixed convection flow near a vertical smooth surface. their study revealed a notable reduction in heat transfer when a moist solution was subjected to a heat source and solute bouyancy, highlighting the complex interplay between these factors. Hussain *et al.* [30] examined the impact of heat transfer on the flow of a Carreau fluid through a stretching cylinder, considering nonlinear stretching rates and non-uniform heat generation/absorption. their research revealed that the combination of heat generation and nonlinear stretching rate disrupts the thermal profile within the fluid, potentially altering blood flow through vessels. in addition, numerous studies have examined the effects of internal non-uniform heat generation/absorption on MHD fluid flow through various mediums, further exploring its characteristics and impact.(see Refs. [31–41]).

Upon reviewing existing literature, a significant knowledge gap was identified. The impacts of magnetic fields and porosity on the temperature of micropolar Casson fluids have not been explored. To address this, the present study aim to model the flow of Casson fluid through a porous linearly stretchy sheet with heat sink/source, incorporating magnetic and porosity terms into the thermal equations and to develop an approx-

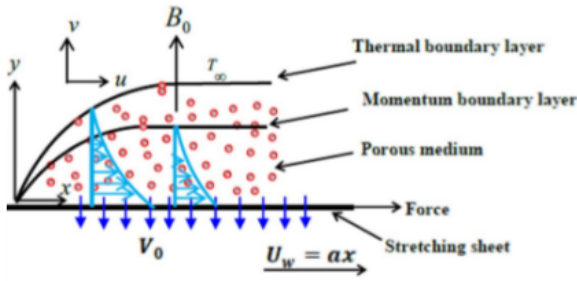


Figure 1: Schematic depiction of the flow.

imate solution using the Hermite Collocation Method(HCM) with Gauss-Lobatto points, making it the first to apply this numerical technique to this specific model. The study will help scientists and engineers to optimize heat transfer management in industries and will lead to more insight into computational technique for complex dynamics of Magnetohydrodynamics(MHD) Casson fluid flow in porous channel

## 2. mathematical formulations

The steady two dimensional flow of a micropolar Casson fluid through a porous medium with permeability  $K_p^*$ , over a horizontal linear stretchy sheet was considered. A uniform transverse magnetic field  $B_0$  is applied, causing the fluid to be electrically conductive. The external flow velocity is given by  $U_e = bx$ , and the stretching sheet moves with velocity  $U_w = ax$ , where  $a$  and  $b$  are positive constants, and  $x$  is the coordinate along the stretchy sheet. Also, the melting temperature is assumed as  $\bar{T}_w$  and the free stream temperature  $\bar{T}_\infty$  of the fluid satisfy  $\bar{T}_w > \bar{T}_\infty$ . The schematic diagram of the flow is depicted in figure 1 below.

The equations governing the model are formulated as follows [44]:

$$\frac{\partial \bar{u}}{\partial x} + \frac{\partial \bar{v}}{\partial y} = 0, \quad (1)$$

$$\bar{u} \frac{\partial \bar{u}}{\partial x} + \bar{v} \frac{\partial \bar{u}}{\partial y} = \nu \left( 1 + \frac{1}{\beta} \right) \frac{\partial^2 \bar{u}}{\partial y^2} - \frac{\sigma^* B_0^2 \bar{u}}{\rho_f} + \left( \frac{k}{\rho} \right) \frac{\partial H}{\partial y} - \frac{\nu}{K_p^*} \bar{u}, \quad (2)$$

$$\bar{u} \frac{\partial H}{\partial x} + \bar{v} \frac{\partial H}{\partial y} = \frac{\gamma}{\rho_j} \frac{\partial^2 H}{\partial y^2} - \frac{k_v}{\rho_j} \left( 2H + \frac{\partial \bar{u}}{\partial y} \right), \quad (3)$$

$$\bar{u} \frac{\partial \bar{T}}{\partial x} + \bar{v} \frac{\partial \bar{T}}{\partial y} = \alpha_1 \frac{\partial^2 \bar{T}}{\partial y^2} - \frac{1}{\rho C_p} \frac{\partial \bar{q}_r}{\partial y} + \frac{Q}{\rho C_p} (\bar{T} - \bar{T}_\infty) + \frac{\nu}{\rho C_p K_p^*} \bar{u}^2 + \frac{\sigma^* B_0^2}{\rho C_p} \bar{u}^2. \quad (4)$$

The boundary conditions for the above eqs. (1), (2), (3), and (4) as follows:

$$\left. \begin{aligned} \bar{u} = \bar{U}_w(x) = cx, \quad \bar{T} = \bar{T}_w, \quad H = 0, \quad \bar{v} = \bar{V}_0 \quad \text{at } y = 0 \\ \bar{u} \rightarrow \bar{U}_e(x) = bx, \quad \bar{T} \rightarrow \bar{T}_\infty \quad \text{as } y \rightarrow \infty \end{aligned} \right\} \quad (5)$$

where  $\alpha_1$  connotes thermal diffusion coefficient of the fluid,  $K_p^*$  indicates the permeability parameter,  $\beta$  denotes Casson fluid parameter,  $(\bar{u}, \bar{v})$  are the velocity components along axes,  $k$  represents the thermal conductivity,  $\sigma^*$  represent electrical conductivity,  $\rho$  is the density of fluid,  $q_r$  represents the Radiative heat flux,  $K_v$  micropolar fluid constant and  $C_p$  is the specific heat capacity.

Considering the Rosseland approximation [42], the Radiative heat flux may be written as:

$$\bar{q}_r = -\frac{4\sigma^*}{3K^*} \frac{\partial \bar{T}^4}{\partial y}, \quad (6)$$

where  $\sigma^*$  denotes the Stefan-Boltzman constant,  $K^*$  represent the mean absorption coefficient, and  $\bar{T}^4$  as expanded adopting Taylor's series as [44].

$$\bar{T}^4 \cong 4\bar{T}_\infty^3 \bar{T} - 3\bar{T}_\infty^3.$$

Below are the similarity transformations used to convert the partial differential equations (1), (2), (3), and (4) into ordinary differential equations:

$$\left. \begin{aligned} \eta = y \sqrt{\frac{b}{\nu}}, \quad \bar{u} = bx f'(\eta), \quad \bar{v} = -\sqrt{b\nu} f(\eta), \\ H = b \sqrt{\frac{b}{\nu}} x g(\eta), \quad \bar{\theta}(\eta) = \frac{\bar{T} - \bar{T}_\infty}{\bar{T}_w - \bar{T}_\infty} \end{aligned} \right\} \quad (7)$$

Putting eq. (7) into eqs. (1), (2), (3), and (4) gives the following:

$$(1 + \beta^{-1}) f'''' + f f'' - f'^2 - (\Omega + M) f' + A_0 g' = 0, \quad (8)$$

$$\lambda_1 g'' + f g' - f' g - A_0 B (2g + f'') = 0, \quad (9)$$

$$f \bar{\theta}' + \left( \frac{1}{Pr} + R \right) \bar{\theta}'' + \Delta \bar{\theta} + Ec (\Omega + M) f'^2 = 0. \quad (10)$$

The transformed boundary conditions associated with the model are stated as follows:

$$\left. \begin{aligned} f(0) = S, \quad f'(0) = \epsilon, \quad \theta(0) = 1, \quad g(0) = 0 \quad \text{at } y = 0 \\ f'(\infty) = 1, \quad g(\infty) = 0, \quad \theta(\infty) = 0 \quad \text{as } y \rightarrow \infty \end{aligned} \right\} \quad (11)$$

The obtained dimensionless thermo-physical parameters are:

$$\begin{aligned} A_0 = \frac{k}{\nu \rho}, \quad M = \frac{\sigma B_0^2}{\rho \nu}, \quad \lambda_1 = \frac{\gamma}{\nu \rho}, \quad B = \frac{\nu}{a}, \\ \Omega = \frac{\nu}{a K}, \quad Pr = \frac{\nu}{a}, \quad \Delta = \frac{Q}{\rho C_p}, \quad Ec = \frac{U_e^2(x)}{C_p (T_w - T_\infty)}, \\ \epsilon = \frac{a}{b}, \quad R = \frac{16 \sigma^* T_w^3}{3 K^* K}, \quad S = -\frac{V_0}{\sqrt{a \nu}}, \end{aligned}$$

where  $A_0$ ,  $M$ ,  $\lambda_1$ ,  $B$ ,  $\Omega$ ,  $Pr$ ,  $\Delta$ ,  $Ec$ ,  $\epsilon$ ,  $R$ ,  $S$ , and  $\beta$  are micro-coupling parameter, magnetic parameter, spin gradient parameter, micro-inertia parameter, permeability parameter, Prandtl number, heat generation parameter, Eckert number, stretchy parameter, radiation parameter, suction parameter, and Casson parameter respectively.

This investigation focuses on two essential physical quantities, the skin friction coefficient ( $Cf_x$ ) and the local Nusselt number ( $Nu_x$ ):

$$\begin{aligned} Cf_x &= \frac{\tau_w}{\rho U_\infty^2}, \\ Nu_x &= \frac{xq_w}{k(T_\infty - T_w)}, \end{aligned} \quad (12)$$

where  $\tau_w = \mu(1 + \beta^{-1})\left(\frac{\partial \bar{u}}{\partial y}\right)_{y=0}$  is denoted as the surface shear stress,  $\mu$  is the viscous dynamic of fluid, and  $q_w = -k\left(\frac{\partial \bar{T}}{\partial y}\right)_{y=0} + \bar{q}_r$  is represented as the surface heat flux.

The Skin friction and Nusselt number can be expressed, using eq. (7) as:

$$Cf_x = \frac{\tau_w}{\rho U_\infty^2} = Re_x^{-\frac{1}{2}} Cf = (1 + \beta^{-1})f''(0). \quad (13)$$

And the local Nusselt number is:

$$Nu_x = \frac{x\bar{q}_w}{k(\bar{T}_\infty - \bar{T}_w)} = Re_x^{-\frac{1}{2}} Nu_x = -(1 + R)\theta'(0), \quad (14)$$

where the local Reynolds number is expressed as  $Re_x = \frac{U_\infty x}{\nu}$ .

### 3. Computational techniques

A weighted collocation method is utilized to solve eqs. (8)-(10) numerically. This technique is based on the interpolation theory of unevenly spaced intervals, where Hermite polynomials are chosen as basis functions to approximate the differential equations within the integral range  $a \leq x \leq b$ . The coefficients of the basis functions are determined from a set of selected shifted Gauss-Lobatto points [43]. Specifically, the functions  $\bar{f}$ ,  $\bar{g}$ , and  $\bar{\theta}$  (where  $\bar{f}$ ,  $\bar{g}$ , and  $\bar{\theta}$  are functions of  $\eta$ ) are employed as basis functions,

$$\bar{f} = \text{HermiteH} \sum_{k=0}^{\infty} a_k \left( \frac{2\eta}{\eta_\infty} - 1 \right), \quad (15)$$

$$\bar{g} = \text{HermiteH} \sum_{k=0}^{\infty} b_k \left( \frac{2\eta}{\eta_\infty} - 1 \right), \quad (16)$$

$$\bar{\theta} = \text{HermiteH} \sum_{k=0}^{\infty} c_k \left( \frac{2\eta}{\eta_\infty} - 1 \right), \quad (17)$$

where  $a_k$ ,  $b_k$ ,  $c_k$  for  $k = 0, 1, 2, \dots, n$  are the unknown coefficients to be determined and  $n$  connotes tolerance parameter, otherwise called truncation order. To derive the system of algebraic equations, the boundary conditions (11) are imposed on the basis functions (15)-(17). Additional system of equations are generated through the residual equations  $f_{res}$ ,  $g_{res}$ , and  $\theta_{res}$ . The residual (error) is computed by substituting the basis functions (15)-(17) into equations (8)-(10) and evaluating at evenly spaced intervals  $-\infty \leq \eta \leq \infty$ . The goal is to find the coefficients  $[a_k, b_k, c_k : k = 0..n]$  that minimize the residue across the integration range. Using Mathematical software, the nonlinear system of algebraic equations is solved to obtain the numerical values of the unknown coefficients. These coefficients are then substituted into the basis solutions (15)-(17) to get the numerical solutions to eqs. (8)-(10) for  $\beta = 1.2$ ,  $M = 1$ ,  $\Omega = 0.2$ ,  $\Delta_1 = 1$ ,  $Ec = 0.5$ ,  $A_0 = 0.5$ ,  $\lambda = 1$ ,  $B = 0.5$ ,  $R = 1$ ,  $\epsilon = 0.6391$ ,  $S = 1$ , and  $n = 15$  is determined as:

$$\begin{aligned} \bar{f}(\eta) &= 1.76248 + 0.0177083 \left( -2 + 4 \left( -1 + \frac{2\eta}{3} \right)^2 \right) + 0.0338931 \\ &\quad \left( -12 \left( -1 + \frac{2\eta}{3} \right) + 8 \left( -1 + \frac{2\eta}{3} \right)^3 \right) - 0.00401929 \\ &\quad \left( 12 - 48 \left( -1 + \frac{2\eta}{3} \right)^2 + 16 \left( -1 + \frac{2\eta}{3} \right)^4 \right) + \dots \\ &\quad - 2.53956 \times 10^{-13} \left( -518918400 \left( -1 + \frac{2\eta}{3} \right) \right) \\ &\quad + 2421619200 \left( -1 + \frac{2\eta}{3} \right)^3 - 2905943040 \\ &\quad \left( -1 + \frac{2\eta}{3} \right)^5 + 1383782400 \left( -1 + \frac{2\eta}{3} \right)^7 \\ &\quad - 307507200 \left( -1 + \frac{2\eta}{3} \right)^9 + 33546240 \left( -1 + \frac{2\eta}{3} \right)^{11} \\ &\quad - 1720320 \left( -1 + \frac{2\eta}{3} \right)^{13} + 32768 \left( -1 + \frac{2\eta}{3} \right)^{15} + 0.99409 \left( -1 + \frac{2\eta}{3} \right), \end{aligned} \quad (18)$$

$$\begin{aligned} \bar{g}(\eta) &= -0.01919 - 0.00748609 \left( -2 + 4 \left( -1 + \frac{2\eta}{3} \right)^2 \right) \\ &\quad + 0.00085488 \left( -12 \left( -1 + \frac{2\eta}{3} \right) + 8 \left( -1 + \frac{2\eta}{3} \right)^3 \right) \\ &\quad - 0.00224828 \left( 12 - 48 \left( -1 + \frac{2\eta}{3} \right)^2 + 16 \left( -1 + \frac{2\eta}{3} \right)^4 \right) \\ &\quad + \dots + 7.8279 \times 10^{-12} \left( -518918400 \left( -1 + \frac{2\eta}{3} \right) \right) \\ &\quad + 2421619200 \left( -1 + \frac{2\eta}{3} \right)^3 - 2905943040 \left( -1 + \frac{2\eta}{3} \right)^5 \\ &\quad + 1383782400 \left( -1 + \frac{2\eta}{3} \right)^7 - 307507200 \left( -1 + \frac{2\eta}{3} \right)^9 \end{aligned}$$

$$\begin{aligned}
& + 33546240 \left(-1 + \frac{2\eta}{3}\right)^{11} - 1720320 \left(-1 + \frac{2\eta}{3}\right)^{13} \\
& + 32768 \left(-1 + \frac{2\eta}{3}\right)^{15} + 0.0340893 \left(-1 + \frac{2\eta}{3}\right), \quad (19)
\end{aligned}$$

$$\begin{aligned}
\bar{\theta}(\eta) = & 0.498253 - 0.0356253 \left(-2 + 4 \left(-1 + \frac{2\eta}{3}\right)^2\right) \\
& + 0.0177887 \left(-12 \left(-1 + \frac{2\eta}{3}\right) + 8 \left(-1 + \frac{2\eta}{3}\right)^3\right) \\
& - 0.000458665 \left(12 - 48 \left(-1 + \frac{2\eta}{3}\right)^2 + 16 \left(-1 + \frac{2\eta}{3}\right)^4\right) \\
& + \dots - 3.32636 \times 10^{-12} \left(-518918400 \left(-1 + \frac{2\eta}{3}\right)\right. \\
& + 2421619200 \left(-1 + \frac{2\eta}{3}\right)^3 - 2905943040 \left(-1 + \frac{2\eta}{3}\right)^5 \\
& + 1383782400 \left(-1 + \frac{2\eta}{3}\right)^7 - 307507200 \left(-1 + \frac{2\eta}{3}\right)^9 \\
& + 33546240 \left(-1 + \frac{2\eta}{3}\right)^{11} - 1720320 \left(-1 + \frac{2\eta}{3}\right)^{13} \\
& \left. + 32768 \left(-1 + \frac{2\eta}{3}\right)^{15}\right) - 0.433684 \left(-1 + \frac{2\eta}{3}\right). \quad (20)
\end{aligned}$$

The solution procedures are iterated for incremental variations in physical parameters. Table 1 validates the accuracy of the employed Hermite collocation method, and the 4th order shooting Runge-Kutta technique, demonstrating perfect agreement with the `bvp4c` reported in [44]. The favorable comparison, as shown in Table 1, confirms the reliability of the results presented in this study, thereby establishing the authenticity of the method.

Table 1: Validation of results for  $-f''(0)$  as  $\Delta_1 = R = Pr = S = 1$ ,  $B = 0.5$ ,  $\epsilon = 0.6391$ , and  $Ec = 0$

$\beta$	M	$\Omega$	$A_0$	$\lambda$	bvp4c [44]	Runge-Kutta 4	HCM
1.2	1.0	0.2	0.5	1.0	0.5697	0.5696	0.5696
1.4	1.0	0.2	0.5	1.0	0.5948	0.5948	0.5948
1.6	1.0	0.2	0.5	1.0	0.6152	0.6153	0.6153
1.0	1.1	0.2	0.5	1.0	0.5501	0.5521	0.5521
1.0	1.5	0.2	0.5	1.0	0.5969	0.5969	0.5969
1.0	1.9	0.2	0.5	1.0	0.6404	0.6404	0.6404
1.0	1.0	0.3	0.5	1.0	0.5501	0.5521	0.5521
1.0	1.0	0.5	0.5	1.0	0.5740	0.5742	0.5742
1.0	1.0	0.7	0.5	1.0	0.5969	0.5969	0.5969
1.0	1.0	0.2	0.7	1.0	0.5363	0.5363	0.5363
1.0	1.0	0.2	0.9	1.0	0.5355	0.5355	0.5355
1.0	1.0	0.2	1.1	1.0	0.5337	0.5327	0.5327
1.0	1.0	0.2	0.5	1.1	0.5379	0.5376	0.5376
1.0	1.0	0.2	0.5	1.4	0.5384	0.5383	0.5383
1.0	1.0	0.2	0.5	1.9	0.5388	0.5388	0.5388

#### 4. Discussion of results

This study has achieved numerical solutions for the nonlinear coupled system of eqs. (8)-(9) through the application

of weighted residual collocation techniques employing Hermite polynomial as basis functions, complemented by 4th-order shooting Runge-Kutta methods as a control mechanism. The results underscore the crucial role of physical terms in shaping velocity, micro-rotation, and energy distributions. In the mathematical simulations, the standard values are prescribed as  $1 < \beta \leq 1.6$ ,  $1 < M \leq 1.9$ ,  $0 < \Omega \leq 0.7$ ,  $1 < Pr \leq 1.7$ ,  $0.5 < Ec \leq 2$ ,  $1 < R \leq 1.8$ ,  $\Delta_1 = \lambda = S = 1$ ,  $A_0 = B = 0.5$ , and  $\epsilon = 0.6391$ . The sensitivity of physical parameters is exhibited in the results summarized in Tables 2-3 [44] and graphically represented in Figures 2-10.

The parametric study presented in Table 2 investigates the influence of  $\beta$ ,  $M$ ,  $\Omega$ ,  $Pr$ ,  $Ec$ , and  $R$  on skin friction. The results indicate that  $\beta$ ,  $M$ , and  $\Omega$  exhibit a negative correlation with skin friction as they are increasing. Also, there is no significant impact on skin friction for the variation of  $Pr$ ,  $Ec$ , and  $R$ . Table 2 summarizes the Nusselt number results for different values of  $\beta$ ,  $M$ ,  $\Omega$ ,  $Pr$ ,  $Ec$ , and  $R$ . Parametric analysis reveals that increments in  $M$ ,  $\Omega$ ,  $Pr$ ,  $Ec$ , and  $R$  induce a decrease in heat transfer rate.

The impact of the Casson parameter ( $\beta$ ) on the  $f'(\eta)$  is delayed in Figure 2, revealing a monotonic decrease in velocity as  $\beta$  increases. The increase in Casson parameter enhances stress and viscosity, hence reduces fluid mobility. Figure 3 illustrates the response of the  $f'$  distribution to an increasing magnetic field ( $M$ ). The plot reveals that escalating  $M$  values lead to a decrease in the  $f'$  profile, attributed to the Lorentz force opposing the fluid flow. Figure 4 presents the effect of varying porosity term ( $\Omega$ ) on the velocity profile. As  $\Omega$  increases, the  $f'(\eta)$  profile decreases, primarily due to the increased permeability of the wall surfaces. This permeability induces a repulsive force, opposing the fluid flow and resulting in a reduced velocity boundary layer thickness.

Figure 5 demonstrates the impact of varying micro-coupling parameter  $A_0$  on the microstructure profile. As  $A_0$  increases, micro-rotation significantly enhances near the lower wall, attributed to the concentration of fragile particle. Conversely, a reverse behavior emerges towards the middle of the channel, progressing toward the top wall. The impact of micro-inertia density  $B$  on micro-rotation is shown in Figure 6, exhibiting enhanced micro-rotation at the lower wall and reduced micro-rotation at the upper wall. Figure 7 shows the effect of spin-gradient viscosity  $\lambda_1$  on micro-rotation near the lower plate but enhances it near the top wall, causing fluid particle movement distortion.

Figure 8 displays the sensitivity of temperature distribution ( $\bar{\theta}$ ) to porosity variations, demonstrating that increased porosity enhances thermal dispersion, reduces thermal resistance, and promotes heat transfer. Figure 9 presents the influence of magnetic field strength ( $M$ ) on temperature distribution  $\bar{\theta}$ . As  $M$  increases, the temperature profile exhibits significant enhancement, primarily as a result of viscous heating, resulting in improved temperature at the wall. Figure 10 displays the thermal profile for various  $Ec$  values, showcasing the impact of viscous dissipation activity parameter. As  $Ec$  increases, the heat profile intensifies due to a constant growth in the heat boundary layer, which unexpectedly reduces viscous dissipation activity. This

conversion of kinetic energy to internal energy is mediated by intermolecular collisions.

Table 2: Analysis of skin friction sensitivity on various parameters for  $\Delta_1 = \lambda = S = 1, A_0 = B = 0.5,$  and  $\epsilon=0.6391$

$\beta$	M	$\Omega$	$P_r$	$Ec$	R	SRK	HCM [ $-f''(0)$ ]	$Cf_x$
1.2	1.0	0.2	0.5	1.0	1.0	0.5696	0.5696	1.0442
1.4	1.0	0.2	0.5	1.0	1.0	0.6062	0.6063	1.0394
1.6	1.0	0.2	0.5	1.0	1.0	0.6368	0.6368	1.0348
1.0	1.1	0.2	0.5	1.0	1.0	0.5521	0.5523	1.1046
1.0	1.5	0.2	0.5	1.0	1.0	0.6532	0.6532	1.3064
1.0	1.9	0.2	0.5	1.0	1.0	0.7430	0.7430	1.4860
1.0	1.0	0.3	0.5	1.0	1.0	0.5521	0.5517	1.1034
1.0	1.0	0.5	0.5	1.0	1.0	0.6042	0.6044	1.2088
1.0	1.0	0.7	0.5	1.0	1.0	0.6532	0.6532	1.3064
1.0	1.0	0.2	1.1	1.0	1.0	0.5247	0.5247	1.0494
1.0	1.0	0.2	1.4	1.0	1.0	0.5247	0.5247	1.0494
1.0	1.0	0.2	1.7	1.0	1.0	0.5247	0.5247	1.0494
1.0	1.0	0.2	0.5	0.7	1.0	0.5251	0.5250	1.5000
1.0	1.0	0.2	0.5	0.9	1.0	0.5251	0.5251	1.5002
1.0	1.0	0.2	0.5	1.1	1.0	0.5251	0.5251	1.5002
1.0	1.0	0.2	0.5	1.0	1.1	0.5247	0.5247	1.0494
1.0	1.0	0.2	0.5	1.0	1.4	0.5247	0.5247	1.0494
1.0	1.0	0.2	0.5	1.0	1.7	0.5247	0.5247	1.0494

$$Cf_x = Re_x^{-\frac{1}{2}} C_f = -(1 + \beta^{-1})f''(0).$$

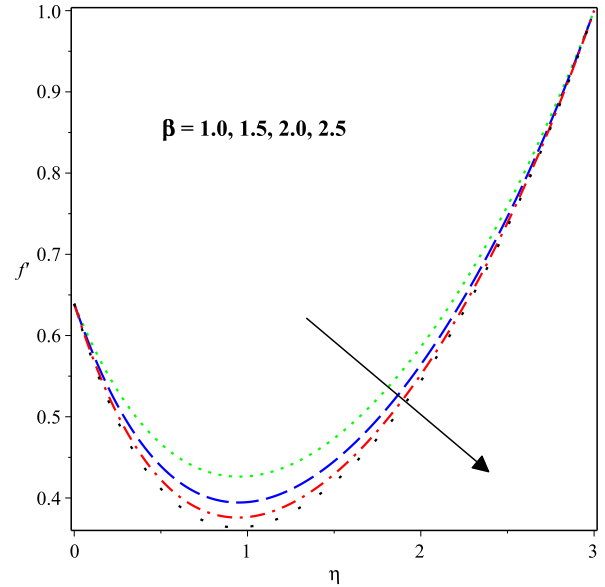


Figure 2: Influence of  $\beta$  on the velocity distribution.

Table 3: Analysis of nusselt number sensitivity on various parameters for  $\Delta_1 = \lambda = S = 1, A_0 = B = 0.5,$  and  $\epsilon=0.6391$

$\beta$	M	$\Omega$	$P_r$	$Ec$	R	SRK	HCM [ $\theta'(0)$ ]	$Nu_x$
1.0	1.0	0.2	0.5	1.0	1.0	-0.0556	-0.0556	-0.1112
1.2	1.0	0.2	0.5	1.0	1.0	-0.0574	-0.0573	-0.1146
1.4	1.0	0.2	0.5	1.0	1.0	-0.0584	-0.0584	-0.1168
1.0	1.1	0.2	0.5	1.0	1.0	-0.0389	-0.0389	-0.0778
1.0	1.5	0.2	0.5	1.0	1.0	0.0182	0.0182	0.0364
1.0	1.9	0.2	0.5	1.0	1.0	0.0632	0.0632	0.1264
1.0	1.0	0.3	0.5	1.0	1.0	-0.0416	-0.0416	-0.0832
1.0	1.0	0.5	0.5	1.0	1.0	-0.0086	-0.0086	-0.0172
1.0	1.0	0.7	0.5	1.0	1.0	0.0182	0.0182	0.0364
1.0	1.0	0.2	1.2	1.0	1.0	-0.0816	-0.0816	-0.1795
1.0	1.0	0.2	1.4	1.0	1.0	-0.1130	-0.1130	-0.2828
1.0	1.0	0.2	1.6	1.0	1.0	0.0086	0.0086	0.0172
1.0	1.0	0.2	0.5	1.0	1.0	-0.0300	-0.0300	-0.0600
1.0	1.0	0.2	0.5	1.5	1.0	0.0089	0.0089	0.0178
1.0	1.0	0.2	0.5	2.0	1.0	0.0661	0.0661	0.1082
1.0	1.0	0.2	0.5	1.0	1.2	-0.0816	-0.0816	-0.1795
1.0	1.0	0.2	0.5	1.0	1.5	-0.1131	-0.1131	-0.2828
1.0	1.0	0.2	0.5	1.0	1.8	-0.1380	-0.1380	-0.3864

$$Nu_x = Re_x^{-\frac{1}{2}} Nu_x = -(1 + R)\theta'(0).$$

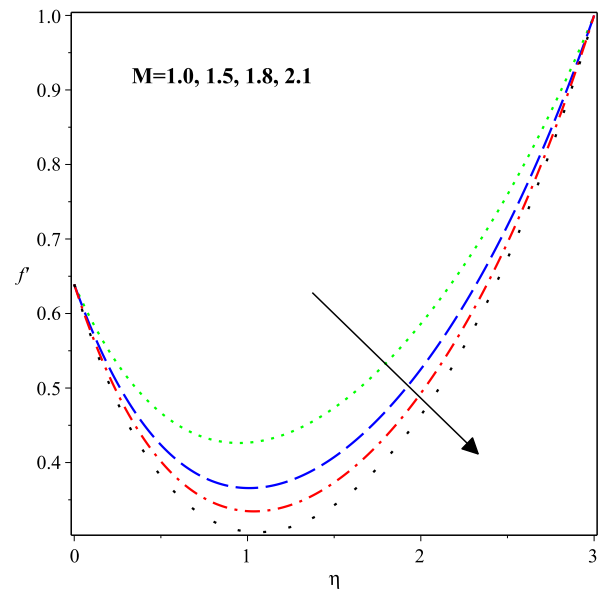


Figure 3: Impact of M on the  $f'(\eta)$ .

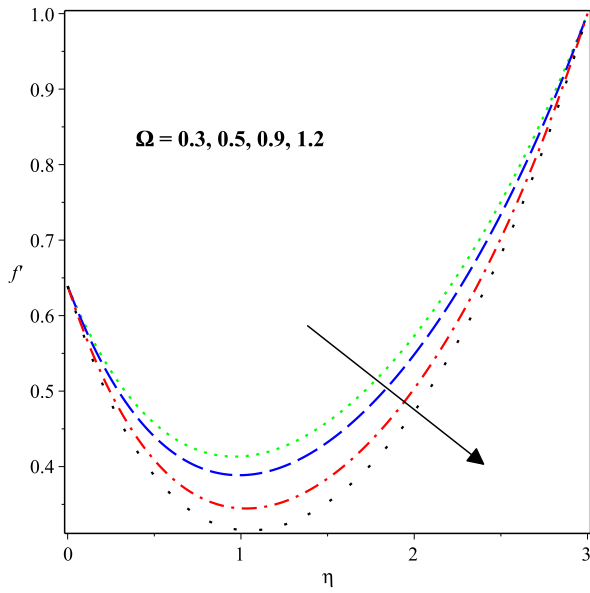


Figure 4: Impact of  $\Omega$  on the  $f'(\eta)$  profile

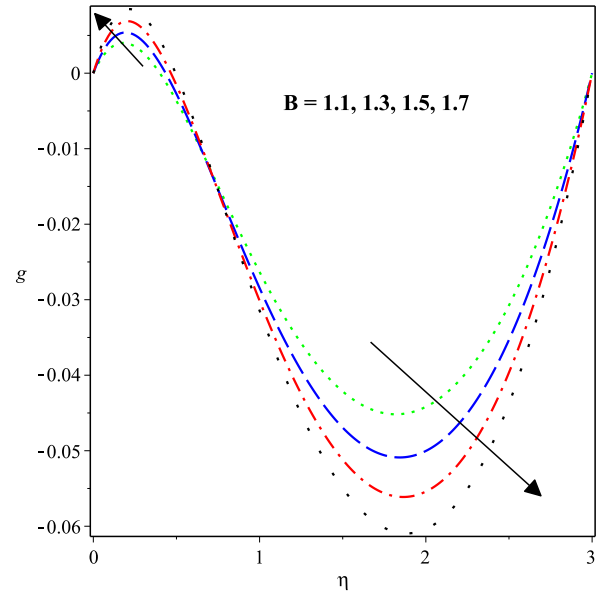


Figure 6: Impact of  $B$  on micro-rotation profile.

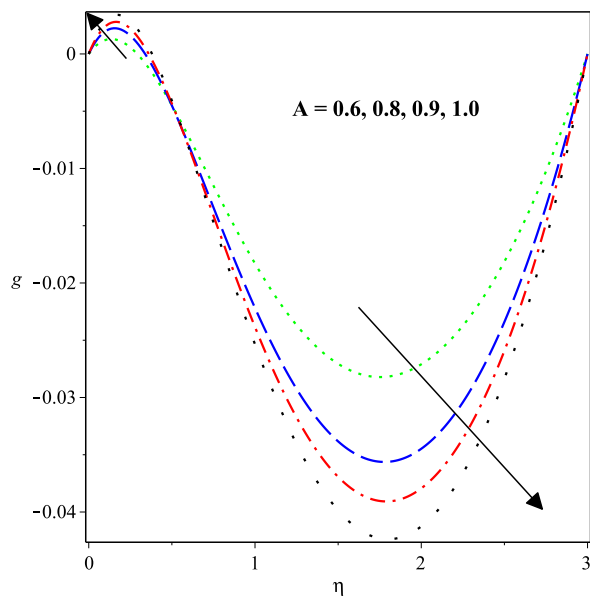


Figure 5: Impact of  $A$  on micro-rotation profile.

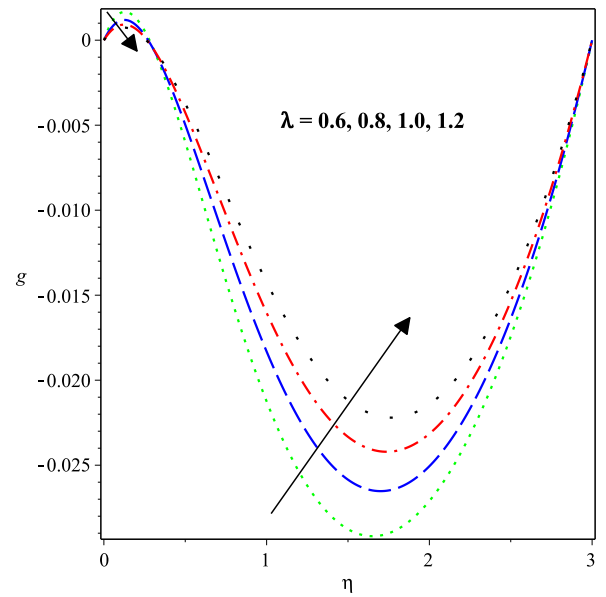


Figure 7: Effect of  $\lambda$  on micro-rotation.

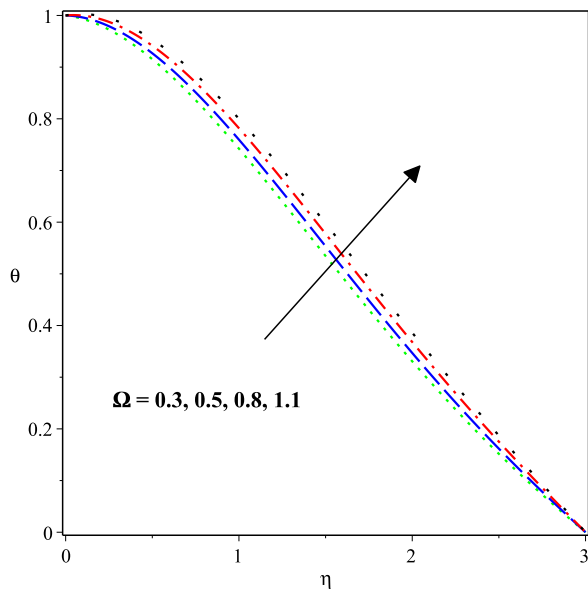


Figure 8: Impact of  $\Omega$  on  $\theta(\eta)$  profile.

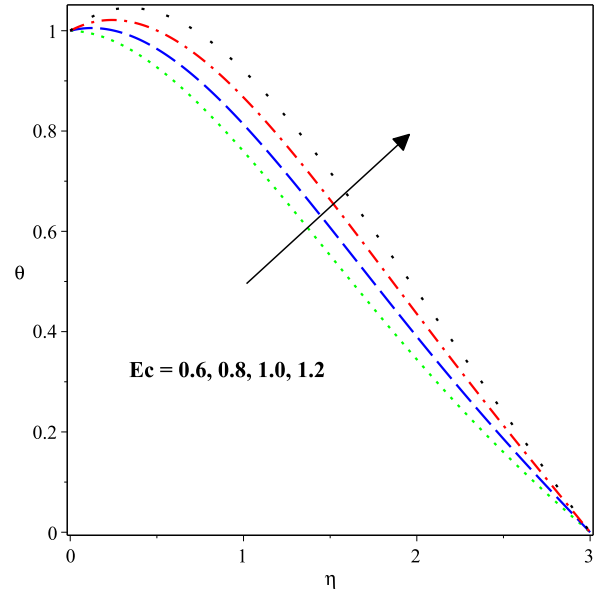


Figure 10: Impact of Eckert number ( $Ec$ ) on Temperature distribution.

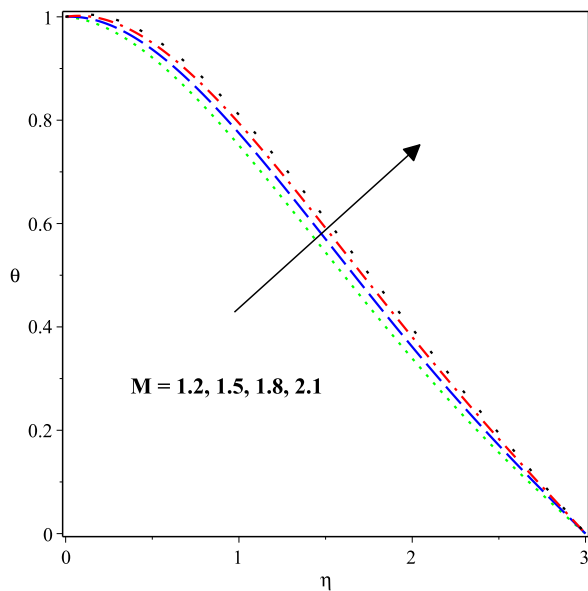


Figure 9: Effect of Magnetic parameter ( $M$ ) on  $\theta(\eta)$ .

## 5. Conclusion

This study numerically examines the magnetohydrodynamic (MHD) flow of micropolar Casson fluid through a porous linearly stretchy sheet with heat sink/source. The fundamental partial differential equations were converted into coupled ordinary differential equations using similarity variables. Numerical solutions were obtained via the collocating weighted residual method, employing Hermite polynomials as basis functions and Gauss-Lobatto points for collocation, alongside a 4th order Runge-Kutta shooting method. The results are presented in tables and plots using Mathematical software. Validation with the existing literature confirms the accuracy and efficiency of the proposed method. A comprehensive analysis of the data reveals several significant findings, including:

- A key discovery from this research is that factors limiting fluid mobility, such as viscosity and permeability, significantly contribute to elevated thermal profiles.
- It is revealed that temperature profile exhibits significant enhancement as the Eckert number parameter increases, indicating a positive correlation.

This research demonstrates the importance of computational analysis in understanding complex fluid flows and heat transfer phenomena, providing valuable insights for experts to boost machine performance by efficiently managing heat transfer through optimized fluid mobility and thermal generation/absorption. The outcomes of this study are particularly relevant to industries where effective heat transfer is critical, such as aerospace, automotive, and energy sectors. Future research directions will concentrate on exploring the impact of nanoparticles on fluid flow behavior.

## Data availability

The data will be available on request from the corresponding author.

## References

- [1] A. J. Benazir, R. Sivaraj & O.D. Makinde, "Unsteady magnetohydrodynamic Casson fluid flow over a vertical cone and flat plate with non-uniform heat source/sink", *Int. J. Eng. Res. Afr.* **21** (2016) 6983. <https://doi.org/10.4028/www.scientific.net/JERA.21.69>.
- [2] S. Shaw, G. Mahanta & P. Sibanda, "Non-linear thermal convection in a Casson fluid flow over a horizontal plate with convective boundary condition", *Alex. Eng. J.* **55** (2016) 1295. <https://doi.org/10.1016/j.aej.2016.04.020>.
- [3] M.G. Sobamowo, "Combined effects of thermal radiation and nanoparticles on free convection flow and heat transfer of casson fluid over a vertical plate", *Int. J. Chem. Eng.* (2018) 7305973. <http://dx.doi.org/10.1155/2018/7305973>.
- [4] T.Hayat, M.B. Ashraf, S.A. Shehzad & A. Alsaedi, "Mixed convection flow of Casson nanofluid over a stretching sheet with convectively heated chemical reaction and heat source/sink", *J. Appl. Fluid Mech.* **8** (2015) 803. <https://doi.org/10.1088/0256-307X/29/11/114704>.
- [5] S.Haldar, S. Mukhopadhyay & G.C. Layek, "Dual solutions of Casson fluid flows over a power law stretching sheet", *J. Appl. Mech. Tech. Phys.* **58** (2017) 629. <https://doi.org/10.1134/S002189441704006X>.
- [6] M. Mustafa & J.A. Khan, "Model for flow of casson nanofluid past a non-linearly stretching sheet considering magnetic field effects", *AIP Adv.* **5** (2015) 077148. <http://dx.doi.org/10.1063/1.4927449>.
- [7] S. Sarkar & M.F. Endalew, "Effects of melting process on the hydromagnetic wedge flow of a casson nanofluid in a porous medium", *Boundary Value Problems* (2019) 114. <https://dx.doi.org/10.1186/s13661-019-1157-5>.
- [8] N. Ibrar, M.G. Reddy, S.A. Shehzad, P. Sreenivasulu & T. Poornima, "Interaction of single and multi walls carbon nanotubes in magnetized-nano casson fluid over radiated horizontal needle", *SN Applied Sciences* **2** (2020) 112. <https://link.springer.com/article/10.1007/s42452-020-2523-8>.
- [9] P.L. Sharma, D. Bains & P. Thakur, "Thermal instability of rotating Jeffrey nanofluids in porous media with variable gravity", *Journal of the Nigerian Society of Physical Sciences*, (2023) 1366. <http://dx.doi.org/10.46481/jnsps.2023.1366>.
- [10] A.K. Kumar, P. Lata, P.L. Sharma, D.B. Bains & P.T. Thakur "Effect of magnetic field on the onset of thermal convection in a Jeffery nanofluid layer saturated by a porous medium: free free, rigid-rigid and rigid-free boundary conditions", *Journal of the Nigerian Society of Physical Sciences*, (2024) 1934. <https://doi.org/10.46481/jnsps.2024.1934>.
- [11] G. Rana & V. Sharma, "Hydromagnetic thermosolutal instability of compressible walters' (model B') rotating fluid permeated with suspended particles in porous medium", *The International Journal of Multiphysics*, **5** (2011) 325. <https://doi.org/10.1260/1750-9548.5.4.325>.
- [12] A.D. Ohaegbue, S.O. Salawu, R.A. Oderinu, A.A. Oyewumi & A.O. Akindele, "Analysis of electromagnetic and radiative heat source on tangential hyperbolic fluid under Arrhenius Kinetic with convective cooling", *International Journal of thermofluids* **23** (2024) 100761. <https://doi.org/10.1016/j.ijft.2024.100761>.
- [13] M.D. Shamshuddin, S.O. Salawu, K. Ramesh, V.S. Patil & P. Humane, "Bioconvective treatment for the reactive casson hybrid nanofluid flow past an exponentially stretching sheet with ohmic heating and mixed convection", *J Therm Anal Calorim* **148** (2023) 1208395. <http://dx.doi.org/10.1007/s10973-023-12465-x>.
- [14] S.A. Lone, M.D. Shamshuddin, S. Shahab, S. Iftikhar, A. Saeed & A.M. Galal, "Computational analysis of MHD driven bioconvective flow of hybrid casson nanofluid past a permeable exponential stretching sheet with thermophoresis and brownian motion effects", *J Magn Mater* (2023) 170959. <https://doi.org/10.1016/j.jmmm.2023.170959>.
- [15] M.D. Shamshuddin, R.P. Sharma, A. Ghaffari, & S.R. Allipudi, "Induced magnetic transportation of soret and dissipative effects on casson fluid flow towards a vertical plate with thermal and species flux conditions", *Int J Mod Phys B* (2023) 2450157. <https://doi.org/10.1142/S0217979224501571>.
- [16] R. Ellahi, S.Z. Alamri & A. Basit, "Effects of MHD and slip on heat transfer boundary-layer flow over a moving plate based on specific entropy generation", *J Taibah Univ Sci* **12** (2018) 476482. <https://doi.org/10.1080/16583655.2018.1483795>.
- [17] M.M. Mousa, M.R. Ali & W.X. Ma, "A combined method for simulating MHD convection in square cavities through localized heating by method of line and penalty-artificial compressibility", *J Taibah Univ Sci*, **15** (2021) 208. <https://doi.org/10.1080/16583655.2021.1951503>.
- [18] K. Maqbool, N. Manzoor & R.S. Ellahi, "Influence of heat transfer on MHD carreau fluid flow due to motile cilia in a channel", *J Therm Anal Calorim* **144** (2021) 2317. <http://dx.doi.org/10.1007/s10973-020-10476-6>.
- [19] F. Selimefendigil & A.J. Chamkha, "MHD mixed convection of AgMgO/water nanofluid in a triangular shape partitioned lid-driven square cavity involving a porous compound", *J Therm Anal Calorim* **143** (2021) 1467. <http://dx.doi.org/10.1007/s10973-020-09472-7>.
- [20] H. Ouri, F. Selimefendigil & M. Bouterra, "MHD hybrid nanofluid convection and phase change process in an L-shaped vented cavity equipped with an inner rotating cylinder and PCM-packed bed system", *Alex Eng J.* **63** (2023) 563. <https://doi.org/10.1016/j.aej.2022.08.016>.
- [21] F. Selimefendigil, H. Chouikhi & H.F. Oztop, "Natural convection and entropy generation of hybrid nanofluid in double annulus separated by a thin rotating partition under magnetic field", *J Magn Mater* **582** (2023) 170974. <https://doi.org/10.1016/j.jmmm.2023.170974>.
- [22] H. Branover & Y. Unger, "Metallurgical technologies, energy conversion, and magnetohydrodynamic flows", *American Institute of Aeronautics and Astronautics* 1993 pp. 32-49 <https://doi.org/10.2514/5.9781600866210.0032.0049>.
- [23] S. Asai, "Magnetohydrodynamics in materials processing", Springer pp. 49-86 2012 [https://doi.org/10.1007/978-94-007-2645-1\\_3](https://doi.org/10.1007/978-94-007-2645-1_3).
- [24] M. Guelman & N. Smirnov, "Magnetohydrodynamic thruster for spacecraft", *Prog Aersp Sci* **83** (2016) 60. <https://doi.org/10.1080/16583655.2023.2271691>.
- [25] S. Kumar, A.J. Chamkha & A.M. Rashad, "Hall current effects on MHD flow in a channel with porous walls", *Results Phys* **21** (2021) 103781. <https://doi.org/10.1016/j.ijft.2020.100061>.
- [26] V. Bojarevics, K. Pericleous & V. Galindo, "Modelling of MHD flow in a liquid metal battery", *J Energy Storage* **30** (2020) 101499. <https://doi.org/10.1080/16583655.2023.2271691>.
- [27] R. Kataria, R.H. Hari & Patel, "Radiation and chemical reaction effects on MHD Casson fluid flow past an oscillating vertical plate embedded in porous medium", *Alexandria Engineering Journal* **55** (2016) 583. <http://dx.doi.org/10.1016/j.aej.2016.01.019>.
- [28] D. Maran, A. Selvaraj, M. Usha & S. Dilipjose, "First order chemical response impact of MHD flow past an infinite vertical plate with in the sight of exponentially with variable mass diffusion and thermal radiation", *Materials Today: Proceedings* **46** (2021) 3302. <https://doi.org/10.1016/j.matpr.2020.11.464>.
- [29] S. Baag, S.R. Mishra, G.C. Dash & M.R. Acharya, "Numerical investigation on MHD micropolar fluid flow toward a stagnation point on a vertical surface with heat source and chemical reaction", *Journal of King Saud University- Engineering Sciences* **29** (2017) 75. <https://doi.org/10.1016/j.jksues.2014.06.002>.
- [30] S.M. Hussain, B.S. Goud, P. Madheshwaran, W. Jamshed, A. A. Pasha, R. Safdar, M. Arshad, R. W. Ibrahim & M. K. Ahmad, "Effectiveness of nonuniform heat generation (sink) and thermal characterization of a Carreau fluid flowing across a nonlinear elongating cylinder: A numerical study", *ACS Omega* **7** (2022) 25309. <https://doi.org/10.1021/acsomega.2c02207>.
- [31] A. Mishra, A. K. Pandey, A. J. Chamkha & M. Kumar, "Roles of nanoparticles and heat generation/absorption on MHD flow of Ag-H<sub>2</sub>O nanofluid via porous stretching/shrinking convergent/divergent channel", *Journal of the Egyptian Mathematical Society* **28** (2020) 17. <https://doi.org/10.1186/s42787-020-00079-3>.
- [32] S. Alao, R. A. Oderinu, E. I. Akinola & O. E. Opaleye, "An alternative method for investigating the effect of squeezing flow of a Casson fluid between parallel walls on magnetic field", *Journal of Mathematical and Computational Science* **12** (2022) 55. <https://doi.org/10.28919/jmcs/6942>.

- [33] D. Gopal, S. H. S. Naik, N. Kishan & C. S. K. Raju, "The impact of thermal stratification and heat generation/absorption on MHD carreau nano fluid flow over a permeable cylinder", *SN Applied Sciences*. **2** (2020) 639. <http://dx.doi.org/10.1007/s42452-020-2445-5>.
- [34] T. Islam, Md. N. Alam, S. Niaza, I. Khan, Md. FayzAlAsad & S. Alqah-tani, "Heat generation/absorption effect on natural convective heat transfer in a wavy triangular cavity filled with nanofluid", *Scientific Reports* **13** (2023) 21171. <https://doi.org/10.1038/s41598-023-48704-2>.
- [35] P.L. Sharma, G.C.Rana & D.Bains, "On Thermal convention in rotating casson nanofluid permeated with suspended particles in a Darcy-Brinkman porous Media" **27** pp. 73-96. <https://doi.org/10.1615/Jpormedia.2024052821>.
- [36] N. H. Hamad, M. Bilal, A. Ali, S. M. Eldin, M. Sharaf & M. Ur Rahman, "Energy transfer through third grade fluid flow across an inclined stretching sheet subject to thermal radiation and Lorentz force", *Scientific Reports* **13** (2023) 19643. <https://doi.org/10.28919/jmcs/6942>.
- [37] S.O. Salawu & E.O. Fatunmbi, "Dissipative heat transfer of micropolar hydromagnetic variable electric conductivity fluid past inclined plate with Joule heating and non-uniform heat generation", *Asian J. Phys. Chem. Sci.* **2** (2017) 110. <https://doi.org/10.9734/AJOPACS/2017/31889>.
- [38] A. M. Obalalu, O. A. Ajala, A. O. Akindele, S. Alao & A. Okunloye, "Effect of melting heat transfer on electromagnetohydrodynamic non-newtonian nanofluid flow over a rigid plate with chemical reaction and arrhenius activation energy", *The European Physical Journal Plus* **136** (2021) 891. <https://doi.org/10.1140/epjp/s13360-021-01869-z>.
- [39] S. Masood, M. Farooq & A. Anjum, "Influence of heat generation/absorption and stagnation point on polystyrene-TiO<sub>2</sub>/H<sub>2</sub>O hybrid nanofluid flow", *Scientific Reports* **11** (2021) 22381. <https://doi.org/10.1038/s41598-021-01747-9>.
- [40] S. Alao, S.O. Salawu, R.A. Oderinu, A.A. Oyewumi & E.I. Akinola, "Investigation of thermal radiation and viscous heating effects on the hydro-magnetic reacting micropolar fluid species flowing past a stretchy plate in permeable media", *International Journal of Thermofluids* (2024) 100600. <https://doi.org/10.1016/j.ijft.2024.100600>.
- [41] S.O. Salawu & A.M. Okedoye, "Thermodynamic second law analysis of hydromagnetic gravity-driven two-step exothermic chemical reactive flow with heat absorption along a channel", *Iran. J. Energy Environ* **9** (2018) 114120. <http://dx.doi.org/10.5829/ijee.2018.09.02.06>.
- [42] S. Rosseland, *Astrophysik, Auf atomtheoretischer grundlage* (1931). <http://dx.doi.org/10.1007/978-3-662-26679-3>.
- [43] M.T. Akolade, T.A. Adeosun & O.J. Olabode, "Influence of thermo-physical features on MHD squeezed flow of dissipative Casson fluid with chemical and radiative effects", *Journal of applied and computational mechanics*, **7** (2021) 1999. <http://dx.doi.org/10.22055/JACM.2020.34909.2508>.
- [44] P. Kumar, B. Singh, S. Goyal, K. Kumar, A. Nandan, K.S. Nisar, S. Alk-hazaleh & Abdel-Aty, "Numerical solution of MHD Micropolar Casson fluid flow over porous linearly stretching sheet with heat source/sink", *Journal of Applied Mathematics and Information Sciences*. **18** (2024) 183. <http://dx.doi.org/10.18576/amis/180118>.